Research on IR Gas Sensor Variable Pressure Environment Compensation and Monitoring Analysis System Based on OLS-WTS Algorithm

Chunguang Wang, Jiahao Su, Yang Liu, Hailong Zhang, Bo Tan, Fuchao Tian

***Abstract*—This paper enhances the precision of industrial gas detection by integrating a pressure compensation algorithm into infrared gas analyzers. We employ a rigorous combination of theoretical analysis and empirical validation to address the deviations in CO_2 (0.5%-4.5%) and CH_4 (2%-18%) detection accuracies observed with three infrared sensors. Our research presents an enhanced soft threshold coupling model based on the least squares-wavelet transform, incorporating data on ambient pressure, test concentrations, and standard gas concentrations. This model significantly reduces errors, surpassing conventional accuracy thresholds. The findings demonstrate the effectiveness of the pressure compensation strategy, providing a robust error optimization framework suitable for varying environmental pressures. This advancement supports the development of in-situ online monitoring systems, thereby enhancing industrial safety and operational efficiency.**

***Index Terms*—infrared spectral sensor, optimized least squares, wavelet analysis, gas online monitoring**

I. Introduction

Accurate monitoring of gases in industrial settings is essential for identifying risks, ensuring safety, and minimizing environmental impact[1]. In various environments, external factors such as gas pressure and temperature can influence sensor accuracy when measuring trace gases, potentially impacting industrial safety and hazard alerts[2]. Variations in atmospheric pressure change the gas quantity per unit volume, altering the spacing between molecules and affecting infrared energy absorption. [3], [4], the concentration of the target gas remains constant, yet the measured concentration can significantly differ from the actual value, necessitating correction for pressure effects[5], [6].

Manuscript received April 27, 2024; revised November 14, 2024. This work was financially supported by the National Natural Science Foundation of China (Grant Nos. 52174229 and 52174230) and the Natural Science Foundation of Liaoning Province (Grant No. 2023-MS- 355，2022-KF-23-03).

Chunguang Wang is a researcher of China Coal Research Institute Fushun Branch, Shenfu Demonstration Zone, 113122, China (e-mail: 13842080243@163.com)

Jiahao Su is postgraduate student of the China Coal Research Institute. Beijing, 100000, China, (e-mail: 15670880885@163.com)

Yang Liu is a researcher of China Coal Research Institute Fushun Branch, Shenfu Demonstration Zone, 113122, China (e-mail: 1066678597 @qq.com)

Hailong Zhang is postgraduate student of the China Coal Research Institute, Beijing, 100000, China, (e-mail: zhl18843668983@163.com)

Bo Tan is a professor of College of Emergency Management and Safety Engineering, China University of Mining and Technology (Beijing), Beijing, BJ 100083, China (e-mail: tanbo709@126.com)

Fuchao Tian is a researcher of China Coal Research Institute Fushun Branch, Shenfu Demonstration Zone, 113122, China (Corresponding author, e-mail: tianfuchao@cumt.edu.cn)

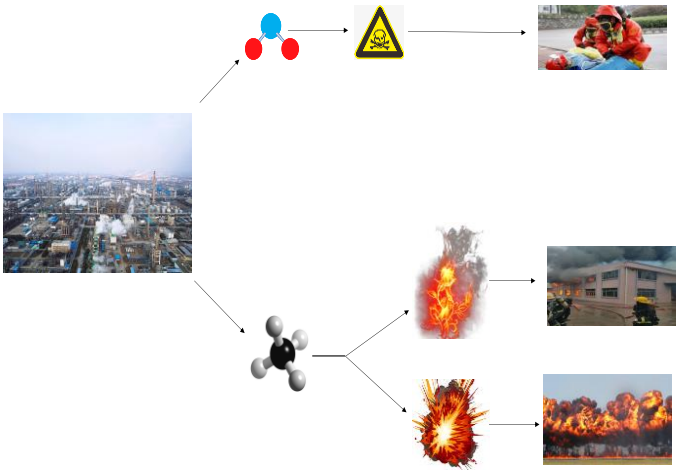

Fig. 1 Pathways and Causes of Gas Leakage in Chemical Parks

Dan et al[7] developed the PSO-WPLS algorithm, a unique hybrid approach for building regression models. This method utilizes the WPT algorithm along with its reconstruction to decompose the acquired spectrum into distinct components. The particle swarm optimization algorithm then selects suitable WPT components based on the prediction error fitness function. Qiulin Tan et al[8] presented a detection system utilizing NDIR technology, which compensates for environmental parameters to simultaneously measure methane, carbon dioxide, and carbon monoxide. Wu Y[9] et al. Proposed a method for compensating temperature drift in pressure sensors through an RBF neural network guided by ant colony clustering. This method utilizes the ant colony algorithm's ability to conduct parallel searches and adaptively modify evaporation coefficients.

Given the scarcity of research on compensating for multiple gases in varying pressure environments, further exploration of current infrared spectral absorption-based pressure compensation methods is necessary[10]. It cannot compensate for errors due to changes in pressure, and its limited scope makes it unsuitable for use in complex and varied environments[11]. Thus, investigating an infrared spectral absorption-based compensation algorithm that is broadly applicable and minimizes errors after adjustment is crucial[12] , is highly significant.

II. Experimental Platform

A. Platform construction

The experiment Platform components included a gas source, TZX-5000A gas dispenser, CO_2 and CH_4 sensors, an industrial control unit, TZX-4000A pressure tester, PC, and related

piping (see Fig. 2).

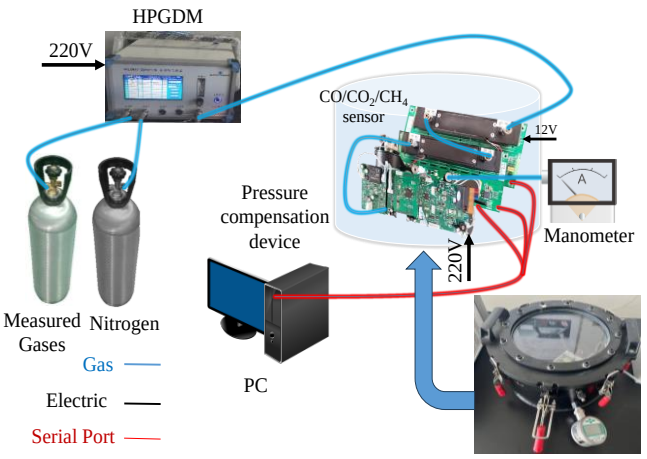

Fig. 2 Experimental platforms

(1) TABLE I lists the specific gas parameters.

TABLE I
GAS PARAMETERS

Gas	Concentration	Background gas	Specification	Properties
Nitrogen（N_2）	99.999%	/	40L	Background gas
Carbon Dioxide（CO_2）	5%	99.999%（N_2）	4L	standard gases
Methane（CH_4）	20%	99.999%（N_2）	4L	standard gases

(2) The TZX-5000A provides an MFC flow rate of 2000 ml in channel 0 and 1000 ml in channel 1. At 25 °C ambient temperature, 31% humidity, and 99.8 kPa pressure, its accuracy ranges from 0.38% to 0.87%, with a consistency of 0.19%.

(3) CO_2 and CH_4 sensors parameters provided in TABLE II.

TABLE II
SENSOR TECHNICAL PARAMETERS

Sensor	Technical principle	Range	Warm-up time	Response time	Output signal	Working power/ power consumption
CO_2	double-beam NDIR detection technique	0-5%	≤20 min	≤30 s	RS-422, RS-485, (4-20) mA	DC12V/≤25 W
CH_4		0-20%	≤20 min	≤30 s		DC12V/≤25 W
CO		0-1,000×10^{-6}	≤30 min	≤60 s		DC12V/25 W; gas cell heating: AC220V/150W

(4) The industrial computer monitors the experimental system's overall operation, providing easy access to parameters like infrared sensor temperatures, concentration data, and detection counts. It ensures coherent information flow and uses precise technical terms, clearly explaining abbreviations where necessary.

(5) The compensation device for ambient pressure consists of two main components: a sealed tank and a suction control box. The sealed tank, which forms the primary structure, includes the tank body and cover, with a capacity of 18.8 L. It operates under external ambient pressures of ±25 kPa, with an additional ±30 kPa pressure component installed on the tank's top for facilitating pressure measurement and regulating both inlet and outlet air interfaces. Connectors link the tank to the pressure measurement device and suction control box, while a digital pressure gauge is included for easy monitoring and adjustment of internal pressure. The system features a sealed tank with a locking mechanism and an observation window. The suction control box contains a shell, a dual-purpose pump, a valve, and an electric control unit. By adjusting the reversing valve, pressure changes in the canister are easily achieved. The shell integrates all components.

B. Experimental methods

The experiment will use infrared sensors with ranges of 0-5% for CO_2 and 0-20% for CH_4, with sensors operating within the pressure compensation device for parallel control[13]. To set up the gas configuration, connect the gas line in series with the TZX-5000A dispenser. Attach the measurement and background gas cylinders, and adjust the inlet flow rate to 300 ml/min[14]. The target gas is mixed with 99.999% N_2 using a high-precision gas distributor to produce different concentrations. Once activated, the gas flows into the pressure compensation device, where its concentration is measured before being discharged through a connected PU pipe. The RS-422 standard, used for data transmission, achieves a rate of 10 MB/s with parallel data lines for improved performance [15]. All three sensor outputs are connected to data terminal equipment (DTE), like PCs, for real-time data transmission, which includes measurements such as absorbance, gas concentration, sensor temperature, and count. This data is used for sensor calibration and accuracy analysis[16].

Constant pressure tests were performed at 45 °C, 31% humidity, and 99.8 kPa using pressure sensors without compensation. Standard gas concentrations for test experiments. CO_2 concentrations ranged from 0.5% to 4.5% in 0.5% increments, while CH_4 concentrations ranged from 2% to 18% in 2% increments. The sensor response time is 0.6 seconds, with a flow rate of 500 mL/min. Multiple repeatability tests were performed to ensure data stability[17].

TABLE III
TANDARD GAS CONCENTRATIONS FOR TEST EXPERIMENTS

Gas	Concentrations of standard gases
CO_2/%	0.5,1,1.5,2,2.5,3,3.5,4,4.5
CH_4/%	2,4,6,8,10,12,14,16,18

The evaluation metric compares measured and actual concentrations, before and after compensation. This metric is optimized using an enhanced least squares model, combined with wavelet transform soft threshold strategies. The approach is illustrated in[18] Fig. 3.

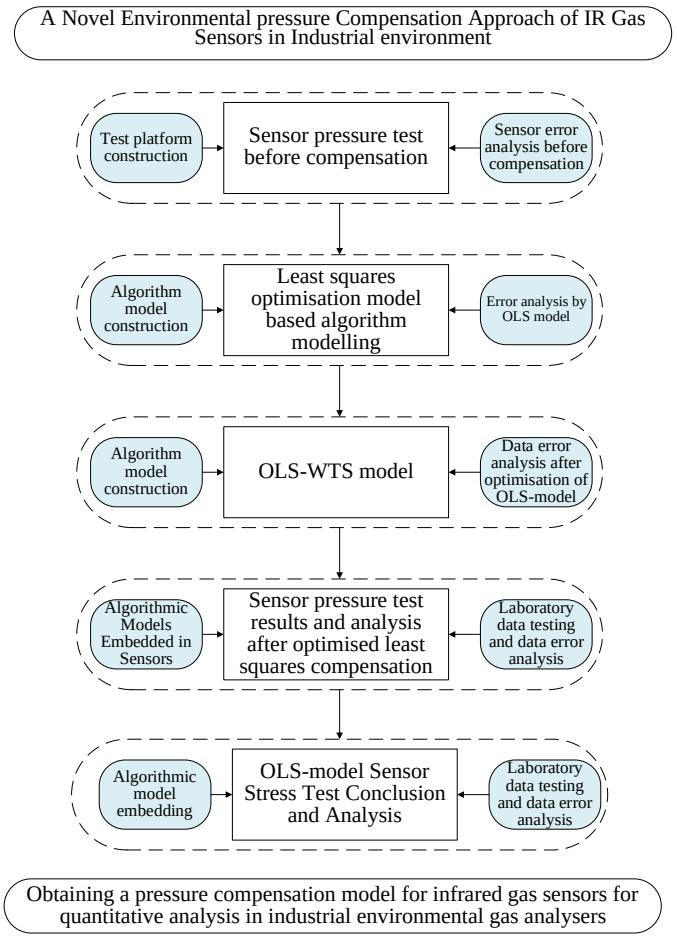

Fig. 3 Experimental procedure

III. Data Analysis

A. *Sensor pressure test results and analysis before compensation*

With the CO_2 sensor range of 0-5%, concentrations of 0.5%-4.5% were tested under varying ambient pressures. Each value Each value is an average of several hundred data points gathered after system stabilization.

TABLE IV
MEASURED DATA BEFORE CO_2 SENSOR COMPENSATION

Pressure	0.5	1	1.5	2	2.5	3	3.5	4	4.5
80 kPa	0.35	0.73	1.03	1.56	1.96	2.58	2.91	3.52	3.87
85 kPa	0.42	0.79	1.13	1.69	2.14	2.73	3.09	3.63	3.98
90 kPa	0.47	0.86	1.22	1.80	2.32	2.88	3.30	3.72	4.12
95 kPa	0.49	0.95	1.31	1.94	2.45	2.99	3.47	3.91	4.31
100 kPa	0.56	1.05	1.41	2.07	2.58	3.11	3.61	4.05	4.45
105 kPa	0.59	1.16	1.55	2.20	2.73	3.24	3.78	4.17	4.56
110 kPa	0.64	1.27	1.64	2.34	2.86	3.33	3.89	4.33	4.67
115 kPa	0.69	1.37	1.75	2.46	2.97	3.47	4.04	4.46	4.87
120 kPa	0.74	1.46	1.88	2.59	3.05	3.59	4.18	4.58	5.01

The table above presents CO_2 gas measurements to examine their trends with respect to ambient pressure at different CO_2 concentrations, along with their absolute error trends.

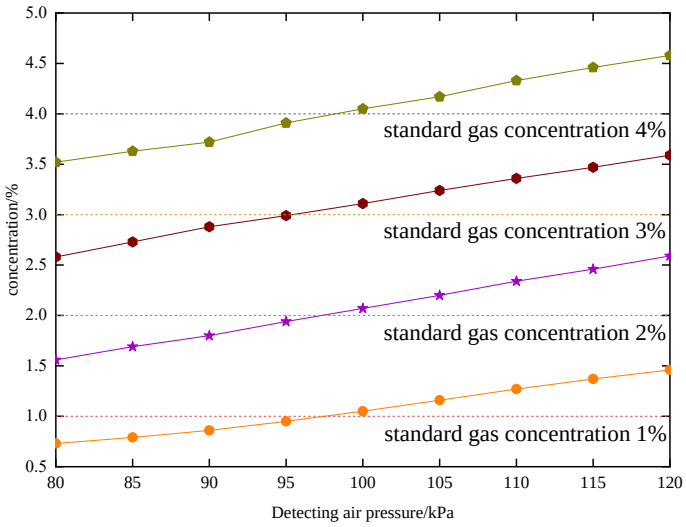

Fig. 4 Variation in detected CO_2 concentration with ambient pressure across different concentration levels

Fig. 4 shows that CO_2 concentration increases with rising ambient pressure. The concentration drops below the standard value when exposed to negative pressure[19], Near-atmospheric pressure produces values closest to the standard, whereas positive pressure generally results in higher concentrations.

TABLE V
MAXIMUM ABSOLUTE ERRORS FOR DIFFERENT STANDARD CO_2 GAS CONCENTRATIONS

Gas concentration /%	0.5	1.0	1.5	2.0	2.5	3.0	3.5	4.0	4.5
Maximum absolute error	0.24	0.46	0.47	0.59	0.55	0.59	0.68	0.58	0.67

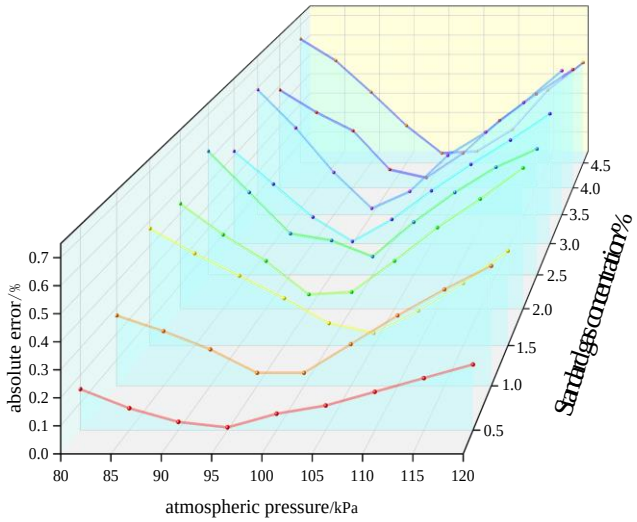

Fig. 5 Trend of CO_2 detection absolute error with ambient pressure across varying concentrations

Fig. 5 illustrates that as the ambient pressure becomes more negative, the absolute error of the infrared CO_2 sensor decreases, thereby enhancing accuracy. Conversely, under positive pressure conditions, increasing ambient pressure leads to greater absolute error, which diminishes detection accuracy[20].

TABLE VI
MEASURED DATA OF MULTIPLE CONCENTRATION POINTS BEFORE COMPENSATION OF CH_4 SENSOR

pressure	0.5 /%	1/ %	1.5 /%	2/ %	2.5 /%	3/ %	3.5 /%	4/ %	4.5 /%
80 kPa	1.27	2.89	5.03	6.96	8.79	10.73	12.82	15.07	16.88
85 kPa	1.48	3.23	5.32	7.28	8.96	10.95	13.17	15.36	17.09
90 kPa	1.68	3.62	5.53	7.49	9.25	11.37	13.39	15.58	17.36
95 kPa	1.89	3.94	5.75	7.76	9.57	11.69	13.72	15.80	17.57
100 kPa	2.09	4.22	6.02	7.98	9.89	12.02	13.97	16.03	17.81
105 kPa	2.20	4.53	6.24	8.21	10.16	12.33	14.22	16.25	18.08
110 kPa	2.43	4.79	6.46	8.39	10.38	12.56	14.48	16.47	18.25
115 kPa	2.65	4.96	6.68	8.61	10.51	12.79	14.70	16.69	18.54
120 kPa	2.89	5.21	6.86	8.83	10.74	12.92	14.93	16.92	18.76

With a sensor range of 0-20%, CH_4 concentrations of 2% to 18% were tested under different pressures. Each value in TABLE IV is the average of hundreds of measurements collected after system stabilization.

Fig. 6 presents the CO_2 concentration trends under different ambient pressures. Fig. 7 illustrates the absolute error between the measured and standard concentrations, allowing analysis of how this error changes with pressure at various concentration levels.

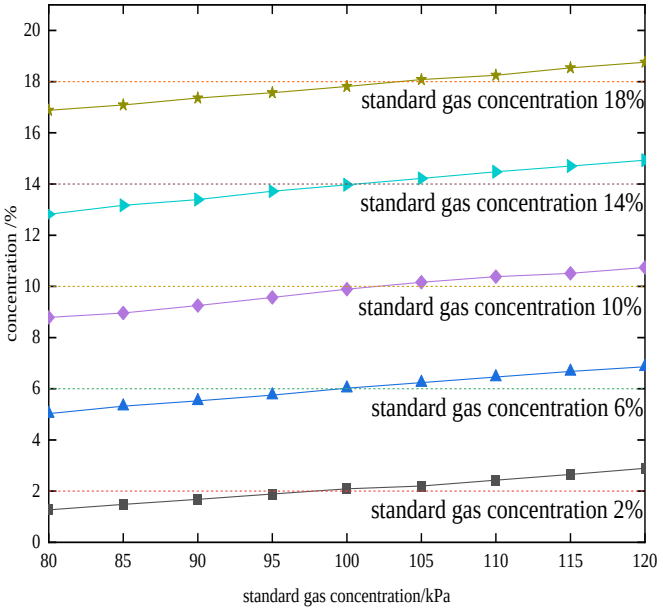

Fig. 6 CH_4 concentration trend with varying ambient pressure at different levels

Fig. 6 indicates that CH_4 concentrations rise as ambient pressure increases. Under negative pressure, the recorded values were mostly below the standard, closest at near-atmospheric levels, and generally higher under positive pressure.

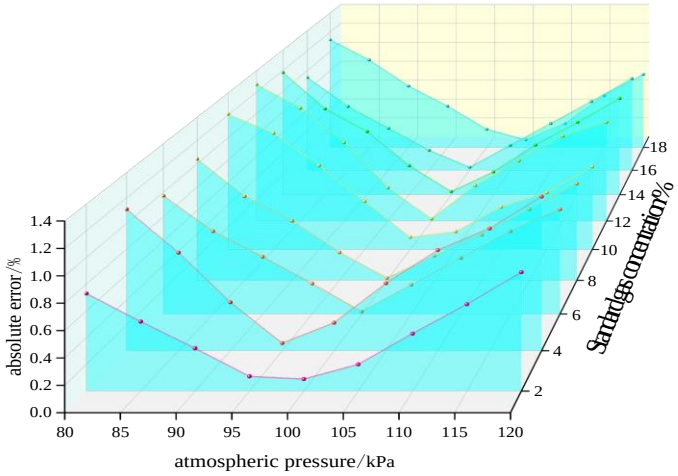

Fig. 7 Absolute error trend in CH_4 detection under different ambient pressures and concentrations.

Fig. 7 shows that under negative pressure, the infrared CH_4 sensor's absolute error decreases as ambient pressure rises, improving accuracy. Conversely, under positive pressure, the error increases, reducing accuracy. TABLE VII shows the maximum absolute errors for CH_4 detection at each concentration level.

TABLE VII
MAXIMUM ABSOLUTE ERRORS FOR DIFFERENT STANDARD CH_4 GAS CONCENTRATIONS

Gas concentration /%	2	4	6	8	10	12	14	16	18
Maximum absolute error	0.89	1.21	0.97	1.04	1.21	1.27	1.18	0.97	1.12

B. Construction of an Optimized Compensation Model Using the Least Squares Method

The three gases' measurement ranges and basic errors meet the technical error standards outlined in TABLE VIII.

TABLE VIII
TECHNICAL SPECIFICATIONS FOR INDUSTRIAL GAS MONITORING SYSTEMS

Gas	Measurement range	Basic error
CO_2	(0～5.0)%	(0～0.5)%：±0.1% ＞0.5%：±(0.075+ True value×5%)
CH_4	(0～100)%	(0～1)%：±0.1% (1～40)%：±True value×10% (＞40～100)%：±10%

Using the experimental data, we developed a mathematical model through least squares optimization. The model involves two steps: first, establishing the relationship between measured concentration and pressure, and second, modeling the true concentration based on the initial output. These steps

help determine concentration errors under different pressures, and an iterative process is used to estimate the true value.

Based on the test data analysis, the impact of ambient pressure changes on the measurement error ΔV is modeled as follows：

$$\Delta V = y = (AX + B)(p_h - p_0) \tag{1}$$

Where *A*, *B* are model parameters; *X* is the measured gas concentration; p_h is the ambient pressure at the site; p_0 is the calibration ambient pressure.

Using the least squares method, the errors corresponding to the same gas concentration at varying pressures are linearly fitted to determine the slope for each gas;

$$\Delta V = (AX + B)(p_h - p_0) \tag{2}$$

Knowing p_0, if $AX + B$ is expressed, then a can be obtained

$$\Delta V = a(p_h - p_0) = ap_h - ap_0 \tag{3}$$

According to the least squares formula, let the equation for fitting a straight line be $y = kx + b$.

The slope of the fitted line is calculated using the least squares method：

$$k = \frac{\sum_i^n xy - n\bar{x}\bar{y}}{\sum_i^n x^2 - n(\bar{x})^2} \tag{4}$$

After calculating the slope *k*, the intercept *b* is determined using the undetermined coefficients method, based on the given points $(\bar{x}, \bar{y})$ [21].

Substituting $\Delta V = y$ and p_h data into equation (3) respectively gives：

$$a = \frac{\sum_i^n p_h \Delta V - n\bar{p}_h \Delta \bar{V}}{\sum_i^n p_h^2 - n(\bar{p}_h)^2} \tag{5}$$

$$A = \frac{\sum_i^n Xa - n\bar{X}\bar{a}}{\sum_i^n X^2 - n(\bar{X})^2} \tag{6}$$

After calculating the value of a, the intercept can be found using the determined points $(\bar{x}, \bar{a})$ and the slope a, applying the method of undetermined coefficients. In equation (1), there are two variables: gas concentration and ambient pressure, with the gas concentration X being the unknown that needs to be solved. Directly solving for *C* is challenging, so the iterative method is employed to approximate its true value. First, establish initial values for the model parameters A, B, and set a maximum allowable error for the true concentration value. Substitute the sensor's actual measured value into equation (1) to determine the error ΔV, If $\Delta V \le K$, falls within the allowable range, the iteration is complete; otherwise, proceed:

$$X = X + \Delta V \tag{7}$$

Substitute equation (7) back into equation (1) to perform further calculations and evaluate the value of ΔV in comparison to K. If the condition $\Delta V \le K$ is met, the iteration is complete; otherwise, the process will be repeated. Since ambient pressure deviations can be both positive and negative, ΔV will also have corresponding positive and negative deviations, which should be carefully considered during iteration to prevent increasing errors.

C. Optimized coupling method of least squares and wavelet transform with soft thresholding

Significant data discrepancies and large fluctuations occur during continuous short-term measurement of three gases[22], This is due to the presence of real gas information along with noise signals from natural radioactive variations in the measurement results[23]. Noise interference causes random changes in rate, amplitude, and phase characteristics, increasing the risk of errors during data processing. This results in data distortion and lowers the quality of valuable information. To solve this, a wavelet system with enhanced analytical capabilities can be applied to reduce noise and improve data accuracy[29]. Multi-resolution wavelet analysis can effectively correct concentration data by reducing noise, thereby enhancing measurement accuracy[25].

Wavelet transform involves shifting a function called the mother wavelet and taking its inner product with the signal X(t) at different scales, denoted as ‘ *a* ’[26], as follows：

$$WT_x(a,\tau) = \frac{1}{\sqrt{a}} \int_{-\infty}^{+\infty} x(t)\varphi^*\left(\frac{t-\tau}{a}\right)dt \tag{8}$$

$$WT_x(a,\tau) = \frac{\sqrt{a}}{2\pi} \int_{-\infty}^{+\infty} x(\omega)\varphi^*(a^{\omega})e^{+j\omega\tau}d\omega \tag{9}$$

The outcome of applying the continuous wavelet transform to the data processed with the optimized least squares model can be described as a function involving the translation factor '*a*' and the scaling factor '*b*'.

$$CWTf(a,b) \leqslant x(t), \psi_{a,b}(t) \geqslant \int_R x(t)\psi^*_{a,b}(t)dt \tag{10}$$

The most important feature of wavelet analysis is its diversity, which allows for the selection of suitable wavelet types for different data curves[25].

In this study, the Daubechies wavelet function, resembling the variation curve of the measured gas concentration, is chosen for data processing. Daubechies wavelets are orthogonal and asymmetrical, commonly denoted as dbN[27], The parameter *N* represents the wavelet order, where higher values lead to improved smoothness and better localization in the frequency domain[28], Typically, *N* ranges from 2 to 10, with N=4used in this study[29], [30].

D. Analysis of Sensor Pressure Test Results After Optimized Least Squares Compensation

The differences between measured and actual CO_2 concentrations at various ambient pressures are calculated using equations (1) and (2), and the results are summarized in TABLE IX.

The optimized least squares method is applied to fit a linear equation between CO_2 concentrations and errors under different pressures, as shown in equations (2) and (3). Each graph, illustrated in TABLE IX, has a minimum fit of 0.97. The slopes of these lines are summarized in TABLE X.

Equations (5) and (6) were used to determine parameters *A* and *B* by applying the optimized least squares method, fitting the slopes of CO_2 concentrations to their actual values. The fitting results are shown in Fig. 9 , with a high degree of fit at

0.9762.

TABLE IX
CALCULATION RESULTS OF ΔV UNDER DIFFERENT AMBIENT PRESSURES FOR DIFFERENT CONCENTRATIONS OF CO_2

P_0	0.5	1	1.5	2	2.5	3	3.5	4	4.5
80kPa	-0.15	-0.27	-0.47	-0.44	-0.54	-0.42	-0.59	-0.48	-0.63
85 kPa	-0.08	-0.21	-0.37	-0.31	-0.36	-0.27	-0.41	-0.37	-0.52
90 kPa	-0.03	-0.14	-0.28	-0.20	-0.18	-0.12	-0.20	-0.28	-0.36
95 kPa	-0.01	-0.05	-0.19	-0.06	-0.15	-0.01	-0.03	-0.09	-0.19
100 kPa	0.00	0.00	0.00	0.00	0.00	0.00	0.00	0.00	0.00
105 kPa	0.09	0.16	0.05	0.20	0.23	0.24	0.28	0.17	0.06
110 kPa	0.14	0.27	0.14	0.34	0.36	0.36	0.39	0.33	0.17
115 kPa	0.19	0.37	0.25	0.46	0.47	0.47	0.53	0.46	0.37
120 kPa	0.24	0.46	0.38	0.59	0.55	0.59	0.68	0.58	0.51

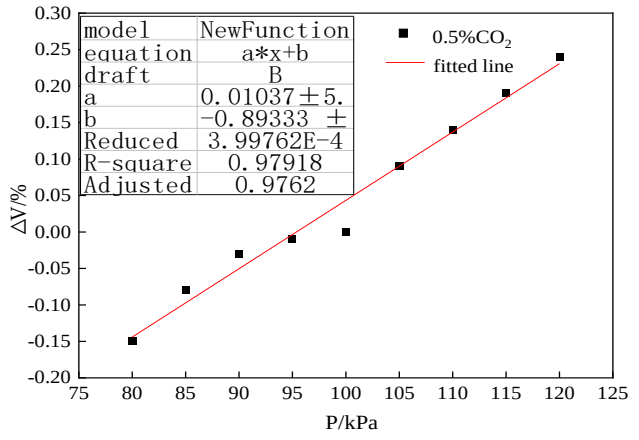

Fig. 8 Straight line fit with error Δv for 0.5% CO_2 gas at different ambient pressures

TABLE X
SLOPE VALUES (DENOTED AS A) FOR VARIOUS CO_2 GAS CONCENTRATIONS ALONG THE STRAIGHT LINE

a	0.01	0.014	0.018	0.023	0.028	0.031	0.033	0.034	0.036
X	0.5%	1.0%	1.5%	2.0%	2.5%	3.0%	3.5%	4.0%	4.5%

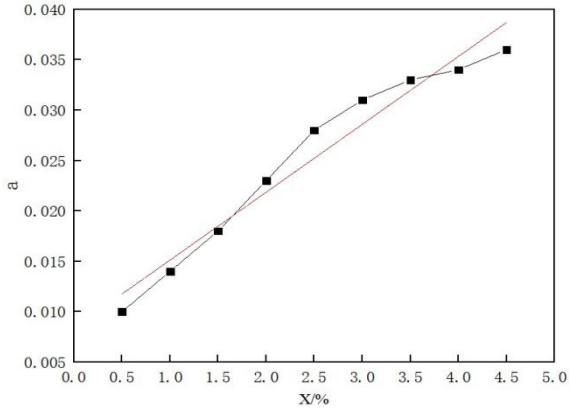

Fig. 9 Straight line fit of the slope of the line a to the actual concentration X for different concentrations of CO_2 gas

From Fig. 9, the parameters are determined as $A=a=0.006$, $B=b=0.008$. Thus, equation (1) can be rewritten as: $\Delta V = (0.006X + 0.008)(p_h - p_0)$, where X is the standard concentration, and P_h and P_0 represent the ambient pressure and calibration pressure, respectively. By substituting the ΔV value into equation (7), the compensated CO_2 concentration is obtained. The resulting values for different ambient pressures are summarized in TABLE XI.

TABLE XI
CO_2 CONCENTRATION VALUES AFTER PRESSURE COMPENSATION

pressure/%	0.5	1	1.5	2	2.5	3	3.5	4	4.5
80 kPa	0.57	1.01	1.37	1.96	2.42	3.10	3.49	4.16	4.57
85 kPa	0.58	1.00	1.39	1.99	2.49	3.12	3.55	4.11	4.51
90 kPa	0.58	1.00	1.39	2.00	2.55	3.14	3.59	4.04	4.49
95 kPa	0.54	1.02	1.40	2.04	2.57	3.12	3.62	4.07	4.49
100 kPa	0.50	1.00	1.50	2.00	2.50	3.00	3.50	4.00	4.50
105 kPa	0.53	1.09	1.46	2.10	2.61	3.11	3.63	4.01	4.38
110 kPa	0.53	1.13	1.47	2.14	2.63	3.10	3.60	4.01	4.32
115 kPa	0.52	1.16	1.49	2.16	2.62	3.08	3.57	3.98	4.34
120 kPa	0.52	1.18	1.54	2.19	2.59	3.07	3.60	3.94	4.31

Similarly, using equations (1) and (2), the difference between measured and true CH_4 concentrations at varying pressures is computed and summarized in TABLE XII.

TABLE XII
CALCULATION RESULTS OF ΔV AT DIFFERENT CONCENTRATIONS OF CH_4 UNDER DIFFERENT AMBIENT PRESSURES

pressure/%	2	4	6	8	10	12	14	16	18
80 kPa	-0.73	-1.11	-0.97	-1.04	-1.21	-1.27	-1.18	-0.93	-1.12
85 kPa	-0.52	-0.77	-0.68	-0.72	-1.04	-1.05	-0.83	-0.64	-0.91
90 kPa	-0.32	-0.38	-0.47	-0.51	-0.75	-0.73	-0.61	-0.42	-0.64
95 kPa	-0.11	-0.06	-0.25	-0.24	-0.43	-0.31	-0.28	-0.20	-0.43
100 kPa	0.00	0.00	0.00	0.00	0.00	0.00	0.00	0.00	0.00
105 kPa	0.20	0.53	0.24	0.21	0.16	0.33	0.22	0.25	0.08
110 kPa	0.43	0.79	0.46	0.39	0.38	0.56	0.48	0.47	0.25
115 kPa	0.65	0.96	0.68	0.61	0.51	0.79	0.70	0.69	0.54
120 kPa	0.89	1.21	0.86	0.83	0.74	0.92	0.93	0.92	0.76

Using equations (2) and (3), the optimized least squares method was applied to fit a linear relationship between the CH_4 concentration and the error Δv caused by pressure variations. Fig. 10 shows that each graph has a minimum fit of 0.98 or higher. The slopes *a* of the fitted lines for various CH_4

concentrations are summarized in TABLE XIII.

TABLE XIII
VALUES OF LINEAR SLOPE A FOR DIFFERENT CONCENTRATIONS OF CH_4 GAS

a	0.039	0.043	0.045	0.046	0.051	0.058	0.061	0.065	0.067
X	2%	4%	6%	8%	10%	12%	14%	16%	18%

Using equations (5) and (6), the optimized least squares method was utilized to fit the slopes of CH_4 concentrations against their respective actual values, thereby determining the model parameters A and B. Fig. 11 displays the fitting results, demonstrating a fit as high as 0.995.

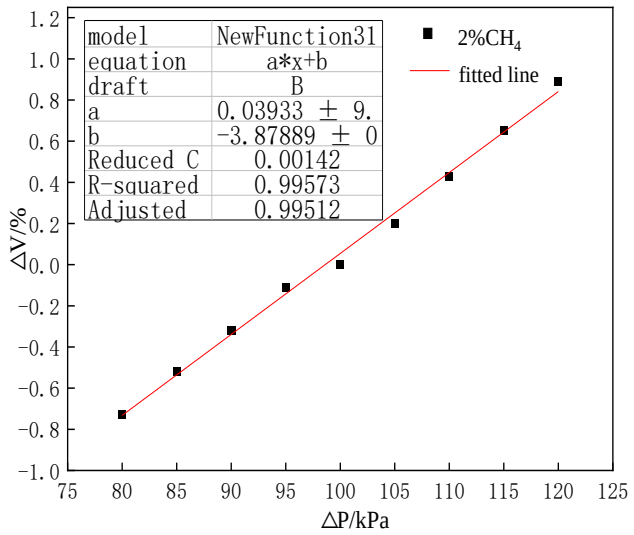

Fig. 10 Linear fit of error Δv for varying CH_4 concentrations under different ambient pressures.

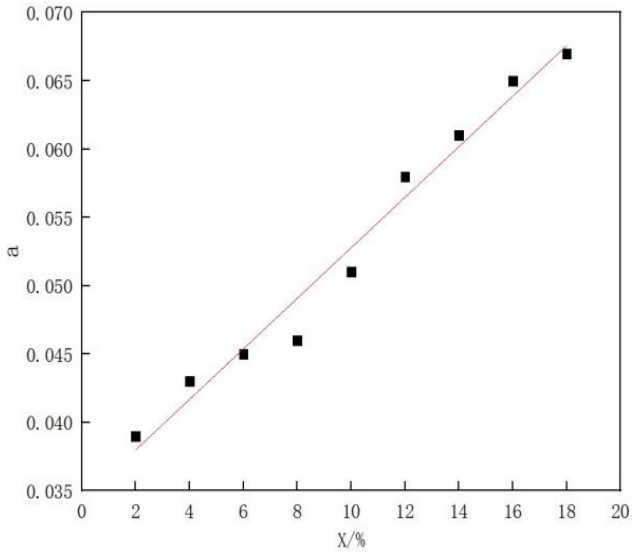

Fig. 11 Straight line fit with error Δv for 2% CH_4 gas at different ambient pressures

The compensated CH_4 concentration values are presented in TABLE XIV.

TABLE XIV
CH_4 CONCENTRATION VALUES AFTER PRESSURE COMPENSATION

pressure/%	2	4	6	8	10	12	14	16	18
80 kPa	2.03	3.73	5.95	7.96	9.87	11.89	14.06	16.39	18.28
85 kPa	2.05	3.86	6.01	8.03	9.77	11.82	14.10	16.35	18.14
90 kPa	2.06	4.04	5.99	7.99	9.79	11.95	14.01	16.24	18.06
95 kPa	2.08	4.15	5.98	8.01	9.84	11.98	14.03	16.13	17.92
100 kPa	2.00	4.00	6.00	8.00	10.00	12.00	14.00	16.00	18.00
105 kPa	2.01	4.32	6.01	7.96	9.84	12.04	13.91	15.92	17.73
110 kPa	2.05	4.37	6.00	7.89	9.84	11.98	13.86	15.81	17.55
115 kPa	2.08	4.33	5.99	7.86	9.70	11.92	13.77	15.70	17.49
120 kPa	2.13	4.37	5.94	7.83	9.66	11.76	13.69	15.60	17.36

From Fig. 11, the parameters are A=a=0.0019, B=b=0.034, Therefore, equation (1) can be rewritten as: $\Delta V = (0.0019X + 0.034)(p_h - p_0)$, where X is the standard concentration, P_h and P_0 represent the ambient pressure and calibration pressure, respectively. The value of ΔV is substituted into equation (7) to calculate the compensated CH4 concentration. The iteration process is repeated until $\Delta V \le K$ where K is the maximum allowable error.

E. Conclusion and Analysis of Sensor Stress Test Using Optimized Least Squares-Wavelet Transform Coupling Model

The optimized least squares compensation model shows significant errors for higher sensor values. In contrast, the wavelet transform's soft thresholding strategy effectively provides accurate compensation for this data.

Unlike the CO_2 analysis method, CH_4 analysis employs the db5 wavelet for decomposition. The Daubechies wavelet used here is orthogonal, has compact support, and can be applied for both continuous and discrete wavelet transforms. The wavelet's support spans 9 units, and it has a filter length of 10. The wavelet function itself is approximately symmetric. Decomposition and reconstruction parameters are identical to those used in the CO_2 data analysis.

The MAE plots in Fig. 14 show the OLS-WTS algorithm and the OLS algorithm for compensating the CO_2 IR Gas Sensor and the CH_4 IR Gas Sensor. The plots show the average absolute error values of different concentrations under different pressure conditions. The OLS-WTS algorithm has a smaller MAE value than the OLS algorithm, but both algorithms stay within the range of 0.20 per cent. The figure shows that the OLS-WTS algorithm's MAE value is significantly smaller than the OLS algorithm, and both algorithms' MAE values remain within 0.20. This indicates that both algorithms' error values are small and within a reasonable range, further demonstrating the superiority of the OLS-WTS algorithm in pressure compensation of the CO_2 IR Gas Sensor.

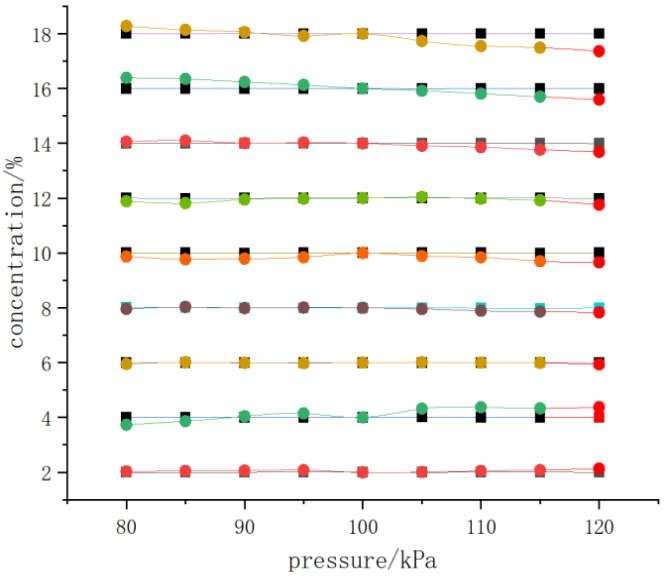

Fig. 12 Standard Gas Concentration Test of CH_4 IR Gas Sensor under Different Atmospheric Pressure Conditions Following OLS-WST Algorithm Embedding

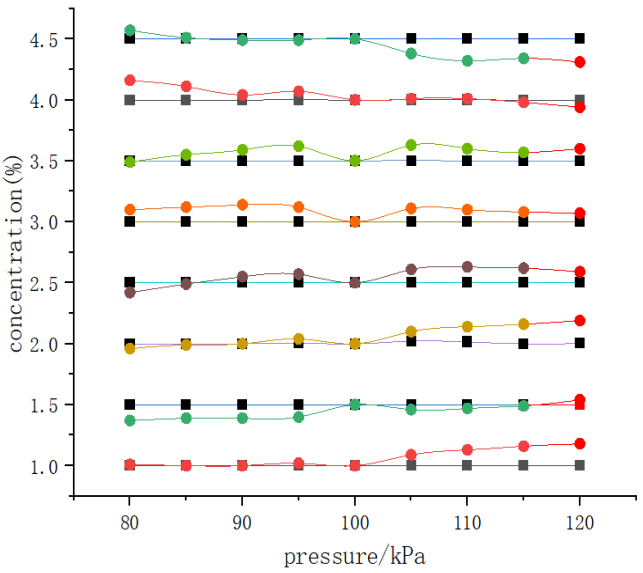

Fig. 13 Standard Gas Concentration Test of CO_2 under Different Atmospheric Pressure Conditions Following OLS-WST Algorithm Embedding

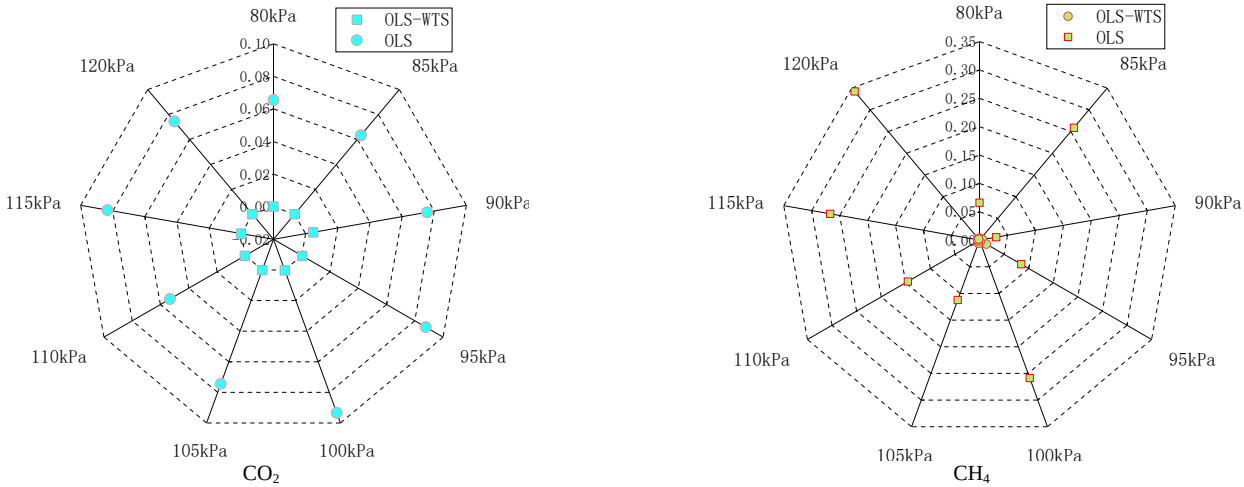

Fig. 14 Compensation of Methane and Carbon Dioxide Sensor MAE Values by OLS-WTS Algorithm and OLS Algorithm under Different Pressure Conditions

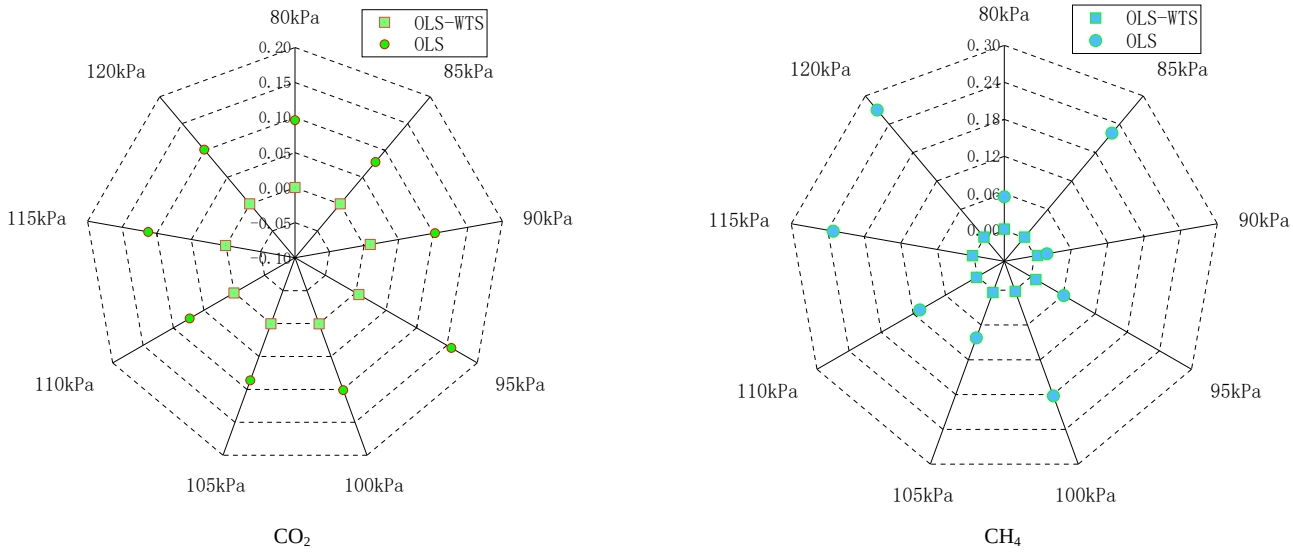

Fig. 15 Compensation of Methane and Carbon Dioxide Sensor RMSE Values by OLS-WTS Algorithm and OLS Algorithm under Different Pressure Conditions

Fig. 15 shows RMSE distribution of the OLS-WTS algorithm and the OLS algorithm when compensating the CO_2 IR Gas Sensor and the CH_4 IR Gas Sensor. The distance from the circle's center to its perimeter represents the RMSE magnitude; a shorter distance to the center signifies a smaller error, and the further away from the center of the circle, the larger the error. The RMSE in the figure ranges from 0.00 to 0.27, indicating that the compensated sensor error is very small and the overall prediction accuracy is high. Most of the data points compensated by the OLS-WTS algorithm are concentrated in the region of lower RMSE (0.0 to 0.05), indicating that the algorithm's compensated error is very small on most of the samples, which makes the compensation effect more satisfactory.

IV. Engineering Applications

The atmospheric pressure compensation model previously discussed was used to enhance the performance of three infrared gas sensors, resulting in the development of t the TZX-1000A on-line multi-gas analysis system designed for industrial applications. This system integrates various pre-processing features, including dust filtration, a sampling pump, a float-type flow regulator, and a precise electronic flow meter. It employs infrared sensors for both CH_4 and CO_2 gases. Additionally, post-processing components such as pressure and temperature sensors, circuit boards, and data analysis software are included to ensure comprehensive monitoring and accurate data processing. This system has been applied in chemical parks for engineering purposes.

A. System performance indicators

Key performance indicators of the TZX-1000A include:
Gas detection module:

TABLE XV
Specifications of the Infrared Gas Sensor Detection Module

Gas type	range	errors
CO	0~1000*10^{-6}	±2% of real value
CO_2	0～5%	(0～0.5)%：±0.1%； ＞0.5%：±(0.075+5% of real value)
CH_4	0～20%	(0～1.00)%：±0.1%； (1.00～20.00)%：±10% of real value

The infrared gas sensor operates in a temperature range from -40°C to 60°C and can handle pressures between 80 kPa and 120 kPa, requiring a 220V power supply. It features B/S mode software for online monitoring and pressure compensation of multiple gases. The system includes a 10" intrinsically safe human-machine interface (HMI) with 12V-DC power and 4G+512M memory with SD offline storage. Additionally, it supports Wi-Fi communication with a range of 300 meters and a speed of 100 Mbps.

B. Practical applications in the field

We deployed the TZX-1000A on-line analyzer at a catalyst company to monitor hazardous gases in the chemical park's daily operations area and verify test accuracy. The device was powered on and warmed up for 30 minutes until data stabilized. We then exported data every 2 minutes, completing eight sets of tests. Results are shown in TABLE XVI. Additionally, gas samples were collected from the test site using gas bags and taken to the laboratory for chromatography analysis to compare gas composition.

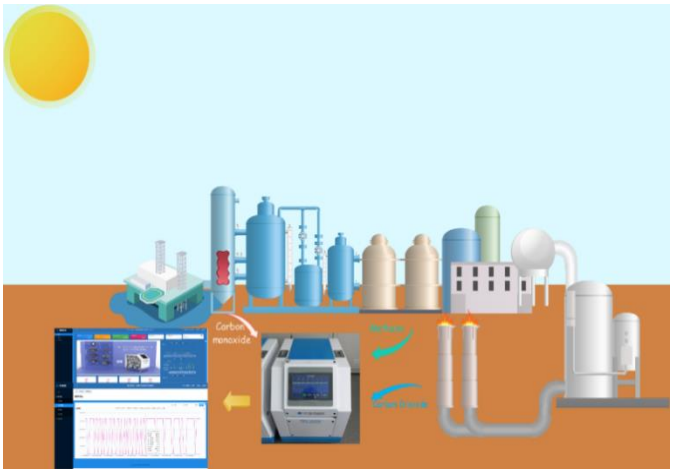

Fig. 16 Application scenarios of the on-line gas monitoring system in an industrial setting

TABLE XVI
Test results of 1# analyzer of SINOPEC Catalysts Co.

Test Method	Gas type	Num							
		1	2	3	4	5	6	7	8
spectral analysis	CO_2/%	0.22	0.31	0.28	0.32	0.238	0.241	0.231	0.242
	CH_4/%	0.021	0.025	0.017	0.031	0.032	0.035	0.027	0.028
Chromatography	CO_2/%	0.221	0.232	0.227	0.235	0.236	0.240	0.230	0.241
	CH_4/%	0.021	0.025	0.017	0.030	0.032	0.036	0.026	0.028
relative error	CO_2/%	0.450	0.433	0.439	1.293	0.840	0.415	0.433	0.413
	CH_4/%	0.000	0.000	0.000	3.226	0.000	2.857	3.704	0.000

Based on eight sets of tests using spectral and chromatographic analysis, the relative error for CO_2 was found to be 0.4-0.9%, and for CH_4, it was 0-4.0%. These results demonstrate that the TZX-1000A analyzer effectively meets the requirements for detecting trace hazardous gases in chemical parks and industrial environments.

V. Conclusion

The accuracy of infrared CH_4 and CO_2 sensors was evaluated using a self-constructed sensor pressure compensation experimental bench within an ambient pressure range of 80kPa to 120kPa. The experimental results indicate that in the 80kPa to 100kPa range, the measured gas concentrations are generally lower than the standard gas concentrations. However, as ambient pressure increases, the absolute error decreases, leading to improved detection accuracy. Near atmospheric pressure conditions, the measured gas concentrations closely match the standard gas concentrations. Conversely, in the 100kPa to 120kPa range, the measured gas concentrations are mostly higher than the standard gas concentrations. As ambient pressure continues to rise, the absolute error increases, resulting in a decline in detection accuracy.

The accuracy of CH_4 and CO_2 gas detection has been improved in most scenarios by employing an optimized least squares pressure compensation model. However, in some specific situations—such as 4.5% CO_2 at 105 kPa, 4.0% CH_4 at 95 kPa, and 400 ppm at 90 kPa—the compensation effect was not ideal, with errors either persisting or slightly increasing after applying compensation. Therefore, further refinements are necessary to enhance the accuracy of gas detection post-compensation.

The analysis reveals that the optimized least-squares (OLS) compensation model produces considerable measurement errors at higher sensor ranges, whereas the wavelet transform soft thresholding (WTS) approach significantly mitigates these errors. In tests conducted on CO_2 infrared gas sensors, the OLS-WTS method consistently achieved mean absolute errors (MAE) of less than 0.20%, surpassing the performance of the OLS model. For CH_4 sensors, using db5 Daubechies wavelet decomposition, the root mean square error (RMSE) for the OLS-WTS method was mostly within the range of 0.0 to 0.05, which is considerably lower compared to the OLS method, demonstrating superior compensation capabilities. Overall, the OLS-WTS model offers enhanced accuracy and reliability in pressure compensation for both CO_2 and CH_4 sensors.

The TZX-1000A on-line analyzer, incorporating the least squares-wavelet transform compensation model, was deployed for monitoring hazardous gases in chemical parks. Field tests were conducted at a catalyst company, with gas samples analyzed in a lab to validate performance. The analyzer showed consistent accuracy, with relative errors ranging from 0.4% to 0.9% for CO_2 and 0% to 4.0% for CH_4. The system offers real-time monitoring, simple operation, rapid analysis, and high accuracy, demonstrating reliability and repeatability, effectively meeting the safety standards for CO_2 and CH_4 detection in industrial environments.

REFERENCES

[1] F. Tian, Y. Liang, H. Zhu, et al, “Application of a novel detection approach based on non-dispersive infrared theory to the in-situ analysis on indicator gases from underground coal fire”, *J. Cent. South Univ.*, Volume 29, Issue 6, Pages 1840-1855, June 2022, doi: 10.1007/s11771-022-5006-9.

[2] Liu Wenqing Opportunities for Development of Optical Monitoring Technologies for the Atmosphere under the "Dual Carbon" Goal, “Journal of Optics”, Vol. 42, No. 6, pp. 0600001, 2022, doi: 10.3788/AOS202242.0600001.

[3] R. Lewicki, M. Jahjah, Y. Ma, et al, “Mid- infrared semiconductor laser based trace gas sensor technologies for environmental monitoring and industrial process control”, Published in SPIE OPTO, M. Razeghi, editor, San Francisco, California, USA, February 2013, pp. 86310W. doi: 10.1117/12.2008701.

[4] M. Jahjah et al, “Atmospheric CH_4 and N_2O measurements near Greater Houston area landfills using a QCL-based QEPAS sensor system during DISCOVER-AQ 2013”, *Opt. Lett*, Volume 39, Issue 4, Page 957, February 2014, doi: 10.1364/OL.39.000957.

[5] X. Zheng, B. M. Chen, “Identification of stock market forces in the system adaptation framework”, *Information Sciences*, Volume 265, Pages 105-122, May 2014, doi: 10.1016/j.ins.2013.12.028.

[6] M. Zolfaghari, M. R. Golabi, “Modeling and predicting the electricity production in hydropower using conjunction of wavelet transform, long short-term memory and random forest models”, *Renewable Energy*, Volume 170, Pages 1367-1381, June 2021, doi: 10.1016/j.renene.2021.02.017.

[7] D. Peng, Q. Nie, Y. Bi, W. Liu, “Particle swarm optimization-based wavelet packet regression for multivariate analysis of near-infrared spectroscopy”, *2012 5th International Conference on Biomedical Engineering and Informatics, BMEI 2012, October 16, 2012 - October 18, 2012*, 2012 5th International Conference on Biomedical Engineering and Informatics, BMEI 2012. Chongqing, China: IEEE Computer Society, 2012, Page 971–975. doi: 10.1109/BMEI.2012.6513066.

[8] Q. Tan et al, “Three-gas detection system with IR optical sensor based on NDIR technology”, *Optics and Lasers in Engineering*, Volume 74, Pages 103-108, November 2015, doi: 10.1016/j.optlaseng.2015.05.007.

[9] Y. Wu, Z. Si, “Application of RBF Neural Network Based on Ant Colony Algorithm in Credit Risk Evaluation of Construction Enterprises”, Revenue 2008 International Conference on Risk Management and Engineering Management, November 2008, pp.653-658.

[10] A. Elia, P. M. Lugarà, C. Di Franco, et al, “Photoacoustic Techniques for Trace Gas Sensing Based on Semiconductor Laser Sources”, *Sensors*, Volume 9, Issue 12, Pages 9616-9628, December 2009, doi: 10.3390/s91209616.

[11] Q. Zhang, Z. Tan, L. Guo, “Compensation of Temperature Drift of MEMS Gyroscope Using BP Neural Network”, December 2009, doi: 10.1109/ICIECS.2009.5365140.

[12] G.-L. Li et al, “Design and Performances of a Carbon Monoxide Sensor Using Mid-Infrared Absorption Spectroscopy Technique at 4.6 μm”, *Spectroscopy Letters*, Vol. 48, No. 6, pp. 454-461, July 2015. doi: 10.1080/00387010.2014.905961.

[13] S. Y. Zhe Li, “High-sensitivity methane monitoring based on quasi-fundamental mode matched continuous-wave cavity ring-down spectroscopy”, *Chin. Phys. B*, Vol. 31, No. 9, pp. 94207-094207, September 2022, doi: 10.1088/1674-1056/ac5d33.

[14] V. Telezhko, M. Tyutchev, M. Averianova, et al “Gas Sensors for Measuring the Concentration of Harmful Substances: Application Features”, *Measurement Techniques*, Volume 64, March 2022, doi: 10.1007/s11018-022-02015-6.

[15] Z. Xiu-lian, Z. Fang, W. Ya-zhe, et al, “Strength prediction model for water-bearing sandstone based on nearinfrared spectroscopy”, *Journal of Mountain Science*, Vol. 20, No. 8, pp. 2388–2404, 2023.

[16] H. Qingsong, et al, “Control System Design and Implementation at Flexible, Distributed Offshore Sensor Test Sites in the Yangtze Estuary Area”, *Journal of Ocean University of China*, Vol. 20, No. 2, pp. 285-295, 2021.

[17] O. Korostynska, A. Mason, A. Al-Shamma’ A, “Microwave sensors for the non-invasive monitoring of industrial and medical applications”, *Sensor Review*, 1981, doi: 10.1108/SR-11-2012-725.

[18] N. Polson, V. Sokolov, J. Xu, “Deep Learning Partial Least Squares”. arXiv, June 26, 2021 . doi: 10.48550/arXiv.2106.14085.

[19] K. A. Smith, R. J. Dowdell, “Gas Chromatographic Analysis of the Soil Atmosphere: Automatic Analysis of Gas Samples For O_2, N_2, Ar, CO_2, N_2O and C_1-C_4 Hydrocarbons”, *Journal of Chromatographic Science*, 1973, doi: 10.1093/chromsci/11.12.655.

[20] C. C. Chi, T. H. Lin, W. C. Huang, et al, “Achievement of high CO_2 concentration in the flue gas at slightly positive pressure during oxy-coal combustion in a 300 kW(th) furnace”, *Fuel*, vol. 160, issue nov.15, 434–439, 2015, doi: 10.1016/j.fuel.2015.08.001.

[21] X. Wang, C. Sun, Y. Yao, et al, “Extension of the definition of tolerance and an application thereof in the calculation of dimension chains”, *International Journal of Advanced Manufacturing Technology*, Vol. 71, No. 5-8, pp. 1069-1076. 2014, doi: 10.1007/s00170-013-5533-5.

[22] Y.-L. Yue, S.-J. Xu, et al, “Nonlinear correction method of pressure sensor based on data fusion”, *Measurement*, Vol. 199, pp. 111303, Aug. 2022, doi: 10.1016/j.measurement.2022.111303.

[23] L. Liu, et al, “Highly sensitive broadband differential infrared photoacoustic spectroscopy with wavelet denoising algorithm for trace gas detection”, *Photoacoustics*, Vol. 21, pp. 100228, Mar. 2021, doi: 10.1016/j.pacs.2020.100228.

[24] O. Hotra, S. Kovtun, O. Dekusha, et al, “Prospects for the Application of Wavelet Analysis to the Results of Thermal Conductivity Express Control of Thermal Insulation Materials”, *Energies*, Volume 14, Issue 17, Page 5223, August 2021, doi: 10.3390/en14175223.

[25] A. K. Alexandridis, A. D. Zapranis, “Wavelet neural networks: A practical guide”, *Neural Networks*, Vol. 42, pp. 1-27, June 2013, doi: 10.1016/j.neunet.2013.01.008.

[26] T. L. Chen, R. Z. You, “A novel fault-tolerant sensor system for sensor drift compensation”, *Sensors and Actuators A: Physical*, Volume 147, Issue 2, Pages 623-632, October 2008, doi: 10.1016/j.sna.2008.05.026.
[27] Simon, H., O., Moss, Keith, Attenborough, “Measurements of the narrow-band decay rates of a gas/particle suspension confined in a cylindrical tube: Relationship to particle concentration”, The Journal of the Acoustical Society of America, Vol. 100, No. 4, pp. 1992–2001, 1996, doi: 10.1121/1.417909.
[28] Wenzhu Huang, Wentao Zhang, Tengkun Zhen, et al , “Phase-Shifted FBG for High-Resolution Static-Strain Measurement Based on Wavelet Threshold Denoising Algorithm”, *J. Lightwave Technol.*, Volume 32, Issue 22, Pages 4294-4300, November 2014, doi: 10.1109/JLT.2014.2354413.
[29] R. Jia, Q. Jiang, “Spectral Analysis of the Transition Operator and Its Applications to Smoothness Analysis of Wavelets”, *SIAM Journal on Matrix Analysis and Applications*, 2002, doi/10.1137/S0895479801397858
[30] Q. Wang, “The shiftability of some wavelet bases”, *Computers & Mathematics with Applications*, Vol. 40, No. 8-9, pp. 957-964, 2000, doi: 10.1016/S0898-1221(00)85006-3.

Chunguang Wang was born in Hebei, China, in 1978. He received the Ph.D. degree from the Henan University of Science and Technology, Jiaozuo, China, in 2019.

He is currently a researcher of the China Coal Research Institute Fushun Branch. His current research interests include Gas Extraction Monitoring.

Jiahao Su was born in Ningxia, China, in 2000. He is currently pursuing the master’s degree with the China Coal Research Institute, Beijing, China.

His research interests include Pressure Sensor Accuracy Compensation Coal Mine Gas Management Technology.

Yang Liu was born in Shandong, China, in 1987. He received the bachelor's degree from the Liaoning Technical University, Fuxin, China, in 2013.

He is currently a researcher of the China Coal Research Institute Fushun Branch. His current research interests include Gas Extraction Monitoring.

Hailong Zhang was born in Jilin, China, in 2000. He is currently pursuing the master’s degree with the China Coal Research Institute, Beijing, China.

His research interests include Industrial environmental gas analysis and monitoring.

Bo Tan ws born in Hunan, China, in 1981. He received the Ph.D. degree from the China University of Mining and Technology (Beijing), Beijing, China, in 2010.

He is currently a Professor of the China University of Mining and Technology. His current research interests include Coal natural mechanism, fire prevention and monitoring technology.

Fuchao Tian was born in Henan, China, in 1984. He received the Ph.D. degree from the China University of Mining and Technology, Xuzhou, China, in 2019.

He is currently a researcher of the China Coal Research Institute Fushun Branch. His current research interests include micro/nanomanufacturing and advanced sensing technology.